

# Infrared Camera (IRC) onboard ASTRO-F (IRIS)

By

Takashi ONAKA\*, Saneyuki FUJITA\*†, Daisuke ISHIHARA\*, Hirokazu KATAZA†,  
Woojung KIM\*‡, Ippei MAEDA†‡, Hideo MATSUHARA†, Toshio MATSUMOTO†,  
Hiroshi MURAKAMI†, Taketoshi NEGISHI\*, Takafumi OOTSUBO\*, Norihide TAKEYAMA\*,  
Kazunori UEMIZU†, Munetaka UENO§, Takehiko WADA†, and Hidenori WATARAI†

(November 1, 2000)

**Abstract:** The Infrared Camera (IRC) is one of the focal-plane instruments on board ASTRO-F (also called as the Infrared Imaging Surveyor; IRIS) and will make imaging and low-resolution spectroscopy observations over a wide spectral range in the near- to mid-infrared from 2 – 26  $\mu\text{m}$ . The IRC will be operated in the pointed observation mode of ASTRO-F to make deep photometric and spectroscopic surveys of wide field-of-views. It will provide a significant database for studies of the formation and evolution of galaxies, properties of brown dwarfs, evolution of planetary systems, and processes of star formation. The IRC comprises three channels: NIR (2 – 5  $\mu\text{m}$ ), MIR-S (5 – 12  $\mu\text{m}$ ) and MIR-L (12 – 26  $\mu\text{m}$ ), and employs state-of-the-art large format array detectors. The NIR channel uses a  $512 \times 412$  InSb array and the MIR channels adopt  $256 \times 256$  Si:As impurity band conduction (IBC) arrays. Each channel has a field-of-view of  $10' \times 10'$  with a nearly diffraction-limited spatial resolution. The NIR and MIR-S channels simultaneously observe the same field on the sky, while the MIR-L observes the sky about  $20'$  away from the NIR/MIR-S position. The design overview and current development status of the IRC are presented.

## 1. INTRODUCTION

ASTRO-F (IRIS: the Infrared Imaging Surveyor), due for launch in early 2004, will be the second Japanese infrared astronomical satellite to be launched with the M-V rocket of the Institute of Space and Astronautical Science (ISAS). It is dedicated for a general sky survey with much better sensitivity than the IRAS survey. The scientific payload consists of a 70-cm cooled telescope of silicon carbide mirrors and two focal-plane instruments, the Infrared Camera (IRC) and the Far-Infrared Surveyor (FIS). The whole scientific payload is installed in a cryostat of 170-liter liquid helium with two 2-stage Stirling cycle coolers (Murakami 1998; Shibai 2000; Onaka 2000).

---

\* Department of Astronomy, School of Science, University of Tokyo, Tokyo 113-0033, Japan;  
onaka@astron.s.u-tokyo.ac.jp

† The Institute of Space and Astronautical Science, Sagami-hara, Kanagawa 229-8510, Japan

‡ Tokyo Metropolitan Institute of Technology, Hino, Tokyo 191-0065, Japan

§ Department of Earth Science and Astronomy, University of Tokyo, Tokyo 153-8902, Japan

ASTRO-F will be brought into a sun-synchronous polar orbit similar to IRAS. The spacecraft spins around the sun-pointed axis once every orbit, pointing the telescope at the zenith. The FIS will perform an all-sky survey in this scanning mode. The IRC is operated in the pointing mode, in which the spacecraft will be fixed in the inertial space and the telescope will be pointed at a target position. A pointed observation may be scheduled up to 3 times per orbit. The duration of one pointed observation is limited to approximately 10 minutes by the condition that the earth should not directly shine on to the cooled baffle of the telescope.

Three phases of the observing program are foreseen. Phase 1 comprises the first 6 months of the mission following the performance verification phase. In phase 1, the far-infrared all sky survey is the primary program and about 1500 pointed observations are planned to be carried out. Phase 2 encompasses the period after phase 1 until the liquid helium exhaustion. It will last approximately 300 days and will have about 7000 pointed observations. In phase 3, the last period, the telescope system will still be kept below 30 K by the Stirling-cycle coolers and only near-infrared observations ( $\lambda < 5 \mu\text{m}$ ) can be carried out. The period of this phase depends on the life time of the coolers, which are now under verification test.

The prime scientific objectives of the IRC range from the observation of the formation and evolution of galaxies in the early universe, the properties of brown dwarfs, the evolution of planetary systems, to the star formation processes by deep photometric and spectroscopic surveys. The IRC has unique characteristics of the wide field-of-view and high spatial resolution with unprecedented sensitivity thanks to the latest large format infrared arrays and the wide spectral coverage owing to the dedicated optical design. Details of the IRC design have been given in Matsuhara (1998), Ueno et al. (1999), and Watarai et al. (2000). In this paper the latest design and the development status are summarized.

Table 1: IRC optics parameters.

Imaging mode

Channel	Filter band ( $\mu\text{m}$ )	PFOV (arcsec)	Array
NIR	1.8 – 2.7; 2.7 – 3.7; 3.7 – 5.1	1.46	512 × 412 InSb
MIR-S	5.5 – 8.5; 8.5 – 13.0; 6.0 – 11.5	2.34	256 × 256 Si:As
MIR-L	12.5 – 18; 18 – 22; 22 – 26	2.34	256 × 256 Si:As

Spectroscopic mode

Channel	Wavelength Range ( $\mu\text{m}$ )	Element	Resolution power ( $\lambda/\Delta\lambda$ )
NIR	2.5 – 5.0	KRS-5 grism	300
	2.0 – 5.0	CaF <sub>2</sub> + Si prism	30
MIR-S	5 – 8	KRS-5 grism	40 – 60
	7 – 12	KRS-5 grism	40 – 60
MIR-L	11 – 19	KRS-5 grism	40
	18 – 26	KRS-5 grism	40

## 2. OPTICAL DESIGN

The IRC consists of three channels: NIR ( $1.8 - 5.0 \mu\text{m}$ ), MIR-S ( $5.0 - 12 \mu\text{m}$ ), and MIR-L ( $12 - 26 \mu\text{m}$ ). All the three channels have the capabilities of wide-field imaging and low-resolution spectroscopy. The parameters of current optical design of each channel are summarized in Table 1. Figure 1 shows the location of the field-of-view of each channel on the focal plane of the telescope. All the three channels have a field of view of  $10' \times 10'$  with a nearly diffraction-limited spatial resolution. The NIR and MIR-S channels share the field-of-view so as to simultaneously observe the same field of the sky. The incident light will be divided by a beam splitter and led to each channel. The MIR-L will observe a field about  $20'$  away from the field of the NIR and MIR-S. Each channel has a filter wheel, in which a blank, three filters, two gratings and/or a prism are installed.

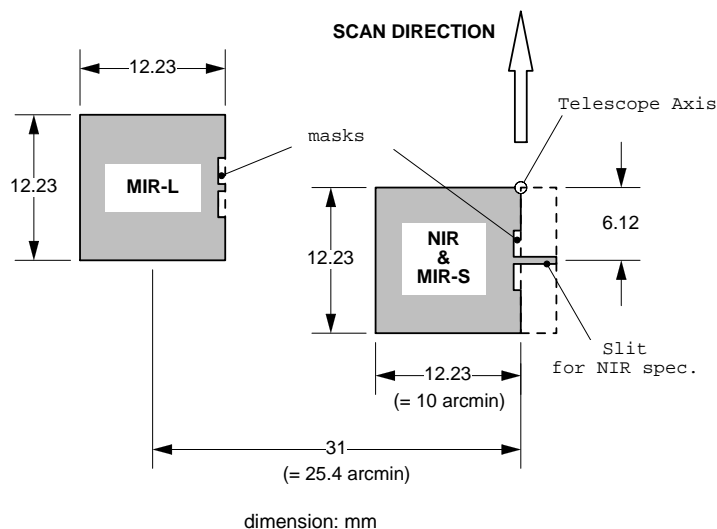


Fig. 1: Field-of-view locations of the three channels of the IRC. The vertical arrow indicates the scan direction in the survey mode.

The NIR channel consists of three spherical Si and one aspherical Ge lenses. The incident near-infrared light ( $< 5 \mu\text{m}$ ) is transmitted through the beamsplitter and is reflected by a pickoff mirror into the NIR channel. A  $512 \times 412$  InSb array is employed for the NIR. Only the  $412 \times 412$  portion is used for imaging with a pixel field of view of  $1.46'' \times 1.46''$ . The extra portion of  $412 \times 100$  pixels will have a slit mask and will be used in the spectroscopic mode (Figure 1). The imaging portion ( $412 \times 412$ ) will also be used for slit-less spectroscopy with the prism or grism.

The MIR-S optics uses two aspherical Ge lenses, while the MIR-L channel consists of a combination of three CsI and two KRS-5 lenses. Both the MIR-S and MIR-L channels will use  $256 \times 256$  Si:As impurity band conduction (IBC) arrays (see section 4). The pixel field of view is  $2.34'' \times 2.34''$ . They will also have small slit masks as shown in Figure 1, which will be used for spectroscopy of extended or diffuse sources. The MIR-S will have a wide-band filter ( $6.0 - 11.5 \mu\text{m}$ ) to aim at a high-sensitivity deep survey. The MIR-L channels will be saturated relatively fast by the source confusion and such a wide-band filter will not be employed (see section 5). The MIR-S and MIR-L will have two gratings to cover their

spectral range with the spectral resolution of about 40. The optical design was required to achieve a good image quality at the operating temperature ( $\sim 6$  K). Refractive indexes of the lens materials at cryogenic temperatures were adopted or estimated from the literature and laboratory experiments (Selvarajan et al. 1979; Hoffman & Wolfe 1991) and have been taken into account in the optical design.

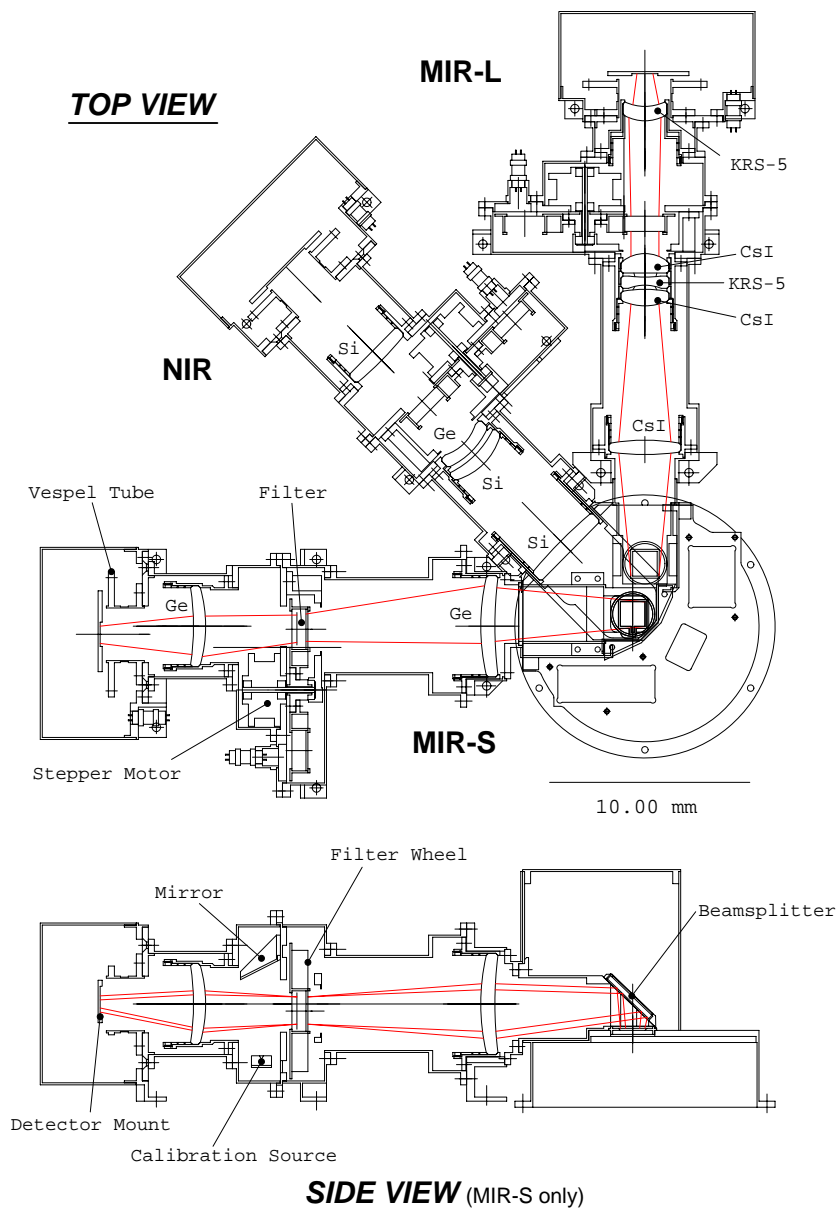


Fig. 2: A top view of the IRC (top) and a side view of the MIR-S (bottom). The optical design for each channel is indicated together with the lens material.

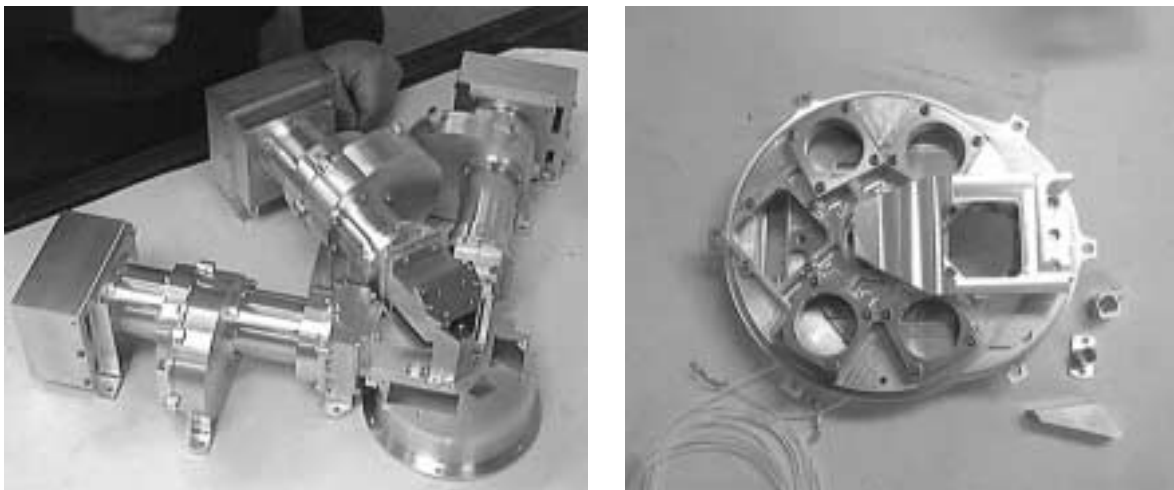


Fig. 3: Photographs of the proto-model of the IRC structure (left) and the NIR filter wheel (right).

### 3. MECHANICAL DESIGN

Figure 2 depicts the final design of the IRC proto-model (PM), while Figure 3 shows photographs of the IRC PM model and the NIR channel filter wheel. All the three channels are joined together to a cylindrical structure, which looks like a Swiss cheese. The Swiss cheese is located at the center of the focal plane and will serve as the alignment basis. The NIR and MIR-S has an anteatr-shape common enclosure near the focal plane to prevent the stray light. Each channel weighs less than 1.2 kg and the current estimate of the total weight of IRC is 3.5 kg.

The filter wheel, the stepper motor, and the calibration light source are all attached to the base plate located near the aperture stop of each channel (Figure 2). The filter wheel is directly driven by the stepper motor specially designed for low-temperature use. The combination of a photodiode and a LED on the wheel housing structure will be used to monitor the filter position. A small ( $30 \mu\text{m} \times 40 \mu\text{m}$ ) resistor made of polysilicon provided by the NASA Goddard Space Flight Center will be used as the internal calibration source to monitor the relative variation in the detector response in a short time scale. The long-term variation will be monitored by measurements of standard stars in the sky. The flat-fielding of the detector response will be made by microscanning observations and laboratory measurements.

### 4. FOCAL-PLANE ARRAYS

State-of-the-art large format infrared arrays, a  $512 \times 412$  InSb array and two  $256 \times 256$  Si:As IBC arrays, manufactured by Raytheon/IRCoE, are employed for the IRC. The InSb and the Si:As IBC detectors are hybridized to the Si multiplexer SBRC-189 and CRC-744, respectively, by indium bumps. Both multiplexers are designed based on the cryo-CMOS technology, which ensures the operation at cryogenic temperatures. The CRC-744 multiplexer has a  $30 \mu\text{m}$  pitch unit cell which consists of three Field-Effect-Transistors (Wu et al. 1997). Laboratory tests have demonstrated good performance of the array at temperatures below 15 K (Table 2). The switched source-follower-per-detector design is adopted for the nondestructive read-out circuit of the pixel voltage. A total of 13 bias voltages are required to operate a CRC-744 multiplexer

with the Si:As detector. The SBRC-189 is a newly designed multiplexer based on the CRC-744 technology with several improvements. The clocking procedure is the same as that of the CRC-744. The total number of biases are reduced to 11 for the InSb array. The SBRC-189 InSb is currently the largest format near-infrared detector array that works at cryogenic temperatures.

All the flight detector arrays including the backups have been mounted on the chip-carriers specially designed for the IRC. The chip carriers are made of ceramic (96 %  $\text{Al}_2\text{O}_3$ ) and the arrays are glued onto the chip-carriers by epoxy resin. Table 2 summarizes the required specifications for the IRC focal-plane arrays and the average performance data of flight detectors provided by Raytheon/IRCoE. The chip-carrier is attached to the fanout board, a glass-epoxy printed circuit, providing the electrical interface to the outside. The IRC housing temperature will be around 6 K in orbit and the optimum temperatures for the detector arrays are slightly higher than the housing temperature, particularly for the NIR array. The array units are thermally isolated from the housing by a Vespel tube and the adjustment of the temperatures of the arrays in appropriate ranges will be made by small heaters on the chip-carrier.

Table 2: Requirement and performance of detector arrays.

InSb  $512 \times 412$  array

Array parameter	Requirement	Average performance
Read noise ( $e^-$ )	$< 20^a$	24.92
Quantum efficiency (%)	80	88.48
Dark current ( $e^-/s$ )	$< 10$	0.2326
Well size ( $e^-$ )		147,000
Operability (%)		99.71
Operating power (mW)	1	0.251

<sup>a</sup> Fowler 4, 60 sec integration

Si:As  $256 \times 256$  IBC array

Array parameter	Requirement	Average performance
Read noise ( $e^-$ )	$< 40^b$	19
Quantum efficiency (%)	40	78
Dark current ( $e^-/s$ )	$< 100$	4.4
Well size ( $e^-$ )		220,000
Operability (%)		99.7
Operating power (mW)	0.5	0.63

<sup>b</sup> Fowler 4, 10 sec integration

## 5. ESTIMATED SENSITIVITIES

Estimated sensitivities in the IRC imaging mode for a single pointed observation are given in Table 3. The detection limit in the table indicates the limit set by the detector and zo-

diacal emission noises. The confusion limits in the near-infrared region are estimated based on the model by Franceschini et al. (1991), while those in the mid-infrared are calculated by new galaxy evolution models by Pearson et al. (2000). In the latter models, two types of the evolutionary scenario are investigated. The first one is the luminosity evolution model, which provides a good fit at bright fluxes to the source counts over a wide range in wavelengths, but may need additional evolution to explain the latest deep ISOCAM survey results (LVOL model). The other one includes the number evolution of ultra-luminous infrared galaxies (ULIRG model). The ULIRG model gives a higher confusion limit than the LVOL model.

The results demonstrate the efficacy of the wide-band filter ( $6 - 11.5 \mu\text{m}$ ) of the MIR-S. The sensitivity will not be limited by the source confusion up to this band width even for the ULIRG model. On the other hand, the source confusion will be a dominant factor for the MIR-L even with the current medium band widths and a wide-band filter will not provide a significant improvement in the sensitivity.

Table 3: Estimated sensitivities of the IRC

Filter band $\mu\text{m}$	Detection limit ( $\mu\text{Jy}$ , $5\sigma$ , 500sec)	Confusion Limit <sup>a</sup> ( $\mu\text{Jy}$ )	
1.8 – 2.7	1		
2.7 – 3.7	1	1	
3.7 – 5.1	2	3	
		LVOL model	ULIRG model
5.5 – 8.5	20	$2.7^b$	$3.3^b$
8.5 – 13	30	$5.2^b$	$7.8^b$
6 – 11.5	17	10.8	17.2
12.5 – 18	85	30	76
18 – 22	120	83	158
22 – 26	150	149	363

<sup>a</sup> For the near-infrared bands the confusion limits are estimated based on the model by Franceschini et al. (1991). The confusion limits in the mid-infrared bands are calculated by Pearson et al. (2000) in two evolutionary models (also see text).

<sup>b</sup> The confusion limits are calculated for slightly narrower band widths than the current design (Pearson et al. 2000).

## 6. CURRENT STATUS

The fabrication of the PM optical elements, such as the lenses, the filters and the beamsplitter, except for the dispersive elements, has been completed and the performance test is being carried out. The fabrication of the CsI lenses may have to be further improved to satisfy the requirements of the figure accuracy, but other lenses have been made satisfactorily within the required accuracy. The final design of the KRS-5 gratings will be fixed based on the performance

test of the verification model.

All the flight detector arrays have been delivered together with engineering-grade (EG) arrays and bare multiplexers. We have measured the basic operation characteristics of the arrays for the bare multiplexers and the EG arrays with the breadboard-model array control electronics (Watarai et al. 2000). The results have confirmed that the required performance can be achieved at the given operating conditions. The flight-model (FM) control electronics will include the improvements to be verified by the measurements currently going on.

The fabrication and integration of the mechanical structure of the PM camera have been completed (Figure 3). The vibration test of the PM structure has been carried out, verifying the current design. The PM digital electronics has been fabricated and the basic interface test with the satellite main computer system has been completed. The FM electronics is being designed and the basic functions will be tested shortly.

The fabrication of the FM IRC will start at the end of 2000 and it will be delivered to the telescope system in the middle of 2001 after the performance test and calibrations.

### ACKNOWLEDGMENT

The ASTRO-F project is managed and operated by the ISAS in collaboration with the groups in universities and institutes in Japan. We are grateful to all the members of the ASTRO-F project for their efforts and help. We thank D. Jennings of Goddard Space Flight Center for providing us the calibration sources and C. Pearson for the estimate of confusion limits based on his new models. H.W. is supported by the JSPS Postdoctoral Fellowship for Young Scientists.

### REFERENCES

- Franceschini, A. et al. 1991, *A&AS*, 89, 285
- Hoffman, J. M. & Wolfe, W. L. 1991, *Appl. Opt.*, 30, 4014
- Matsuhara, H. 1998, *SPIE Proc.*, 3354, 915
- Murakami, H. 1998, *SPIE Proc.*, 3356, 716
- Onaka, T. 2000, in: *ESA SP-456, Proc. of ISO beyond the peaks* (Noordwijk: ESA), in press
- Pearson, C. P. et al. 2000, *MNRAS*, submitted (astro-ph/0008472)
- Selvarajan, A. et al. 1979, *Appl. Opt.*, 18, 3116
- Shibai, H. 2000, *AdSpR*, 25, 2273
- Ueno, M. et al. 1999, *SPIE Proc.*, 3698, 612
- Watarai, H. et al. 2000, *SPIE Proc.*, 4013, 59
- Wu, J. et al. 1997, *Rev. Sci. Inst.*, 68, 3566